5-1970

A Study of The Secant Law for Sporadic E

Ruey-Yuan Han
Utah State University

A STUDY OF THE SECANT LAW FOR SPORADIC E

by

Ruey-Yuan Han

A thesis submitted in partial fulfillment
of the requirements for the degree

of

MASTER OF SCIENCE

in

Electrical Engineering

Approved:

UTAH STATE UNIVERSITY
Logan, Utah

1970

ACKNOWLEDGMENT

The author wishes to express appreciation to:

Dr. Ronney D. Harris for his direction and assistance in this research,

The members of the Antenna and Propagation Laboratory for their cooperation,

His parents, Chin-Tung Han and Chan-Chin Chen, and his wife, Hsiao-Yen Liu, for their encouragement,

The National Science Foundation, for support of the research,

Mrs. C. W. Lauritzen, for editorial assistance.

Ruey-Yuan Han

Ruey-Yuan Han

TABLE OF CONTENTS

LIST OF TABLES

LIST OF FIGURES

LIST OF FIGURES (Continued)

NOTATION

E_s	sporadic E layer or patches.
VI	vertical ionosonde.
BS	backscatter sounder.
$h'E_s$	virtual heights of E_s patches measured from ionogram.
$h_r E_s$	real height of E_s patches.
h'	virtual height of reflection of radio wave.
h_r	real height of reflection of radio wave.
D	distance between the backscatter sounder and ground backscattering area.
ϕ_o	incident angle.
ϕ_W, ϕ_T	incident angles of the oblique incident waves from Wakkanai and Tokyo, respectively.
k_W, k_T	correction factors in the secant law for the curved ionosphere, from the directions of Wakkanai and Tokyo, respectively.
$f_o E_s$	critical frequencies of E_s measured from VI ionogram.
$f_b E_s$	blanketing frequencies of E_s measured from VI ionogram.
f_x	fixed frequency used by Wakkanai and Tokyo backscatter sounders (27.7 MHz).
f_v	frequencies of vertical incidence wave.

f_{oW}, f_{oT} equivalent oblique frequencies from Wakkanai and Tokyo, respectively, corresponding to $f_o E_s$ measured over Akita.

$$f_{oW} = k_W (f_o E_s) \sec \phi_W$$

$$f_{oT} = k_T (f_o E_s) \sec \phi_T$$

f_{bW}, f_{bT} equivalent frequencies similar to f_{oW} and f_{oT}, but corresponding to $f_b E_s$ instead of to $f_o E_s$.

ABSTRACT

A Study of The Secant Law for Sporadic E

by

Ruey-Yuan Han, Master of Science

Utah State University, 1970

Major Professor: Dr. Ronney D. Harris
Department: Electrical Engineering

The secant law is the relationship between the frequencies of a vertically incident wave and an obliquely incident wave that are reflected from the same level (i.e., density) of a stratified ionosphere. This thesis investigates the validity of the secant law applied to sporadic E.

Sporadic E data from two backscatter sounders and one vertical incidence ionosonde located in Japan were studied to test the validity of the secant law. The B-scan photos of the backscatter sounders were searched for E_s patches which were then compared with the sporadic E parameters defined for vertical incidence ionograms.

Finally, two theoretical density models of E_s were analyzed to predict the type of returns expected from the signals of backscatter sounder and vertical incidence ionosonde. These models included the partial reflection and scattering mechanisms that might be appropriate for sporadic E.

(62 pages)

CHAPTER I

INTRODUCTION

Objective and scope

Two backscatter sounders at Wakkanai and Tokyo, Japan, and one vertical ionosonde at Akita surveyed simultaneously a common area of the ionosphere. Four months of sporadic E(E_s) data from these three ionospheric sounders were analyzed. The purpose of this analysis was to determine whether the secant law is valid for sporadic E.

In Chapter I the vertical incident ionosonde and the backscatter sounder are described. The derivation of the secant law is developed in Chapter II for the cases of both flat and curved ionosphere and ground. The results are used in Chapter III to analyze and compare the backscatter and vertical incidence data. The "visibility of E_s" is defined for BS sounders, and then the backscatter and vertical incidence data are compared to obtain the reliability of application of the secant law to sporadic E. Chapter IV discusses theoretically the validity of the secant law for two different sporadic E models. Chapter V summarizes the results of the study and indicates possible further investigation.

Description of vertical ionosonde and backscatter sounder

The vertical incidence ionosonde, VI, is the most common type of radio sounder used to measure the parameters of the ionosphere. It utilizes

a variable exploring frequency (1-25 MHz), and is designed to measure the total travel time of a pulse of radio energy that has been reflected from the ionosphere. A picture of the echo versus frequency is called an ionogram, and is illustrated in Figure 1. This plot can be analyzed by means of the magnetoionic theory to give a profile of electron density versus height.

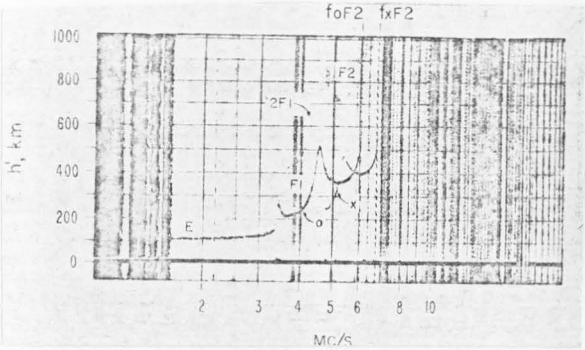

Figure 1. Ionogram of vertical ionosonde.

The rotating backscatter sounder, BS, is a radar device of fixed frequency which transmits radio pulses obliquely to the ionosphere. Over-dense electron patches cause the wave to be reflected back towards the earth. The irregular ground terrain backscatters some of the energy back along the same path to the BS sounder. The resulting echo is displayed on an oscilloscope, usually B-scan, with the ordinate corresponding to azimuthal position of the

antenna and the abscissa corresponding to range in kilometers, as shown in Figure 2. A sporadic E patch thus appears on the backscatter indicator just like a target on a typical radar receiver.

Figure 2. B-scan photo of backscatter sounder.

CHAPTER II

DEVELOPMENT OF THE SECANT LAW

The ionosphere is a partially ionized gas of sufficient density to bend HF radio waves. At frequencies above approximately 1 mc the heavy ions are incapable of responding to the electromagnetic field; therefore, any coupling between the wave and the plasma takes place through the electrons. The net influence of the electrons in the plasma can be described by an equivalent dielectric polarization

$$P = -\frac{Ne^2}{m\omega^2} E$$

in which

N = the electron density,

e = the electronic charge,

m = the electronic mass,

E = the electric field,

ω = the frequency of the wave.

The corresponding electric displacement field can be written

$$D = \mu^2 \epsilon_o E$$

in which ϵ_o is the permitivity of free space, and μ is the refractive index given by

$$\mu = \sqrt{1 - \left(\frac{\omega_N}{\omega}\right)^2} = \sqrt{1 - \left(\frac{f_N}{f}\right)^2} \qquad (2\text{-}1)$$

The plasma frequency is defined by $f_N = \sqrt{\frac{Ne^2}{4\pi^2 \epsilon_o m}}$

If the ionosphere is stratified into homogeneous horizontal layers, Snell's law of refraction can be applied at each boundary to determine the refraction of radio waves between each two homogeneous layers. For a flat ionosphere, the form of Snell's law is

$$\mu_n \sin \phi_n = \mu_{n+1} \sin \phi_{n+1} \tag{2-2}$$

where ϕ is the ray direction with respect to the normal of the layer. The subscripts refer to the layers. Application of Equation (2-2) at each boundary between the free space at which $\mu_o = 1$, and the level of reflection at which $\phi_{n+1} = \frac{\pi}{2}$, yields n + 1 equations. Intermediate values of μ and ϕ can be eliminated from these equations to give

$$\mu_{n+1} = \sin \phi_o \tag{2-3}$$

where ϕ_o is the incident angle at the lower boundary. Usually the subscript of μ in Equation (2-3) is dropped with the understanding that μ is the value of the refractive index at the level of reflection. Substituting Equation (2-1) into Equation (2-3) gives the equation,

$$f = f_N \sec \phi_o \tag{2-4}$$

Equation (2-4) has the interpretation that if ϕ_o is the incidence angle and f_N is the electron density (plasma frequency) at some altitude, f is the

radio wave frequency that will be reflected at that level. If $\phi_o = 0$, $f_N = f_v$, which is the frequency of reflection at vertical incidence. If $\phi_o \neq 0$, Equation (2-4) shows that the operating f can be greater than f_v. The relationship between the oblique f and f_v is called the secant law or

$$f = f_v \sec \phi_o \tag{2-5}$$

The secant law of Equation (2-5) was derived in the absence of any magnetic field. The earth's ionosphere is, however, permeated by the geomagnetic field. If the influence of the magnetic field is considered in the description of the ionospheric plasma, two wave solutions are obtained, each solution corresponding to a different value of the refractive index. Equation (2-6) gives the values of the two refractive indices as functions of electron density and magnetic field (3).

$$\mu = \left[1 - \frac{2X(1 - X)}{2(1 - X) - Y_T^2 \pm \sqrt{Y_T^4 + 4(1 - X)^2 Y_L^2}} \right]^{1/2} \tag{2-6}$$

$$X = \frac{Ne^2}{\epsilon_o m\omega^2} = \left(\frac{f_N}{f}\right)^2$$

$$Y_T = \frac{eB_T}{m\omega}$$

$$Y_L = \frac{eB_L}{m\omega}$$

The quantities B_L and B_T are, respectively, the longitudinal and transverse components of the geomagnetic field with respect to the direction of wave

propagation. Equation (2-6) reduced to Equation (2-1) when $B_T = B_L = 0$. At each level, two values of μ are obtained by inserting the electron density of that level into Equation (2-6). These two refractive indices in turn correspond to two ray paths, which are called the ordinary wave (ray) and the extraordinary wave (ray). There are two values of electron density for which $\mu = \sin \phi_o$, one for each ray. This means that the two rays are reflected at different electron densities or at different levels, as illustrated by the solid curves in Figure 3.

Sporadic E usually appears to have a very sharp vertical gradient of electron density. Thus the reflection levels of the ordinary and extraordinary rays are approximately at the same height. For radio frequencies close to the maximum E_s critical frequency, the ordinary and extraordinary rays are almost coincident. This phenomenon is illustrated by the dotted curves in Figure 3. For this reason the influence of the geomagnetic field is often neglected in the application of the secant law to E_s.

The geometry of an obliquely reflected radio wave is shown in Figure 4. The angle ϕ_o is obtained from the triangle ABT, in which

$$\sec \phi_o = \frac{BT}{BA} = \frac{\sqrt{h'^2 + d^2}}{h'}$$

In this case, both the ground and the ionosphere are taken as parallel infinite planes, which is approximately true for short transmission distances. For greater accuracy, the curvature of the earth and the ionosphere must be taken into consideration, especially when the transmission distance, D, is large.

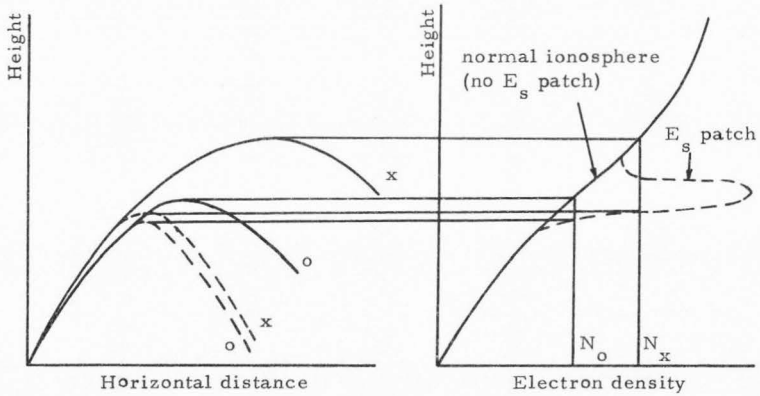

(a) ray paths of oblique reflection (b) electron profile

N_x: the electron density at which μ_x (the refractive index of extraordinary wave) = $\sin \phi_o$

N_o: the electron density at which μ_o (the refractive index of ordinary wave) = $\sin \phi_o$

Figure 3. Reflection of ordinary ray (0) and extraordinary ray (x) from different levels of various electron densities.

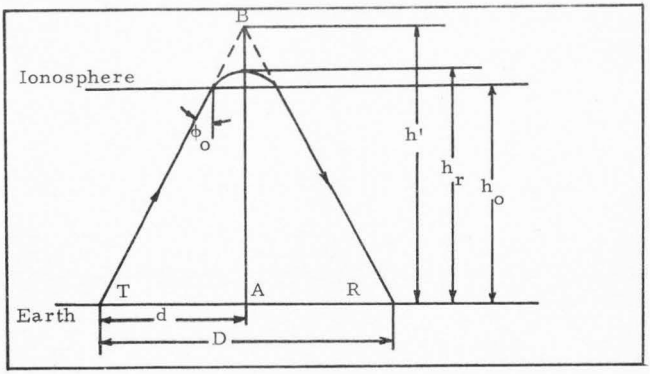

Figure 4. Ray path of oblique incidence for both plane earth and ionosphere.

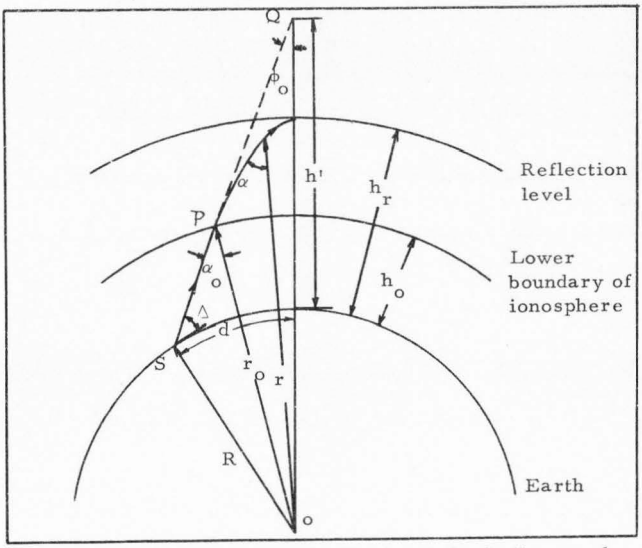

Figure 5. Ray path of oblique incidence for both curved earth and ionosphere.

In the case of both curved ionosphere and ground, Snell's law takes the form

$$\mu r \sin\alpha = \mu_o r_o \sin\alpha_o \tag{2-7}$$

where μ, r, α are the index of refraction, radius from the center of earth and the angle between the ray path and the radius, respectively. See Figure 5.

When the lower boundary of the ionosphere is the reference level, $\mu_o = 1$, $r_o = R + h_o$ (R is the radius of earth, 6371 km, and h_o is the height of the lower boundary) Equation (2-7) can be written

$$\mu r \sin\alpha = (R + h_o) \sin\alpha_o \tag{2-8}$$

At the real height of reflection, h_r, $\alpha = \frac{\pi}{2}$, $r = R + h_r$. Substituting into Equation (2-8)

$$\mu = \left(\frac{R + h_o}{R + h_r}\right) \sin\alpha_o \tag{2-9}$$

According to the law of sines, the triangle OSQ of Figure 5 yields

$$\frac{R}{\sin\phi_o} = \frac{R + h'}{\sin\left(\frac{\pi}{2} + \Delta\right)} = \frac{R + h'}{\cos\Delta} \tag{2-10}$$

and from the triangle OSP,

$$\frac{R}{\sin\alpha_o} = \frac{R + h_o}{\sin\left(\frac{\pi}{2} + \Delta\right)} = \frac{R + h_o}{\cos\Delta} \tag{2-11}$$

Angle $\triangle$ is the elevation angle of the ray path. Eliminating $\cos \triangle$ from Equations (2-10) and (2-11), $\sin \alpha_o$ is given by

$$\sin \alpha_o = \left(\frac{R + h'}{R + h_o} \right) \sin \phi_o \tag{2-12}$$

where ϕ_o is the vertex angle of the straight ray path to the virtual height of reflection. When Equations (2-1) and (2-12) are combined with Equation (2-9)

$$\sqrt{1 - \left(\frac{f_N}{f} \right)^2} = \left(\frac{R + h'}{R + h_r} \right) \sin \phi_o$$

or

$$f_N = f \sqrt{1 - \left(\frac{R + h'}{R + h_r} \right)^2 \sin^2 \phi_o} \tag{2-13}$$

For vertical incidence, $\phi_o = 0$, $f = f_v$ and $f_N = f_v$. If these conditions are inserted into Equation (2-13), the equivalent formula of the secant law for curved earth and ionosphere is given by

$$f = \frac{f_v}{\sqrt{1 - \left(\frac{R + h'}{R + h_r} \right)^2 \sin^2 \phi_o}} \tag{2-14}$$

This formula is not practical since h_r is not measurable by the usual methods, and its value is dependent upon the shape of the electron profile. Equation (2-14) can be used, however, as the starting point for a usable and practical approximation. The factor $\left[(R + h') / (R + h_r) \right]^2$ can be written

$$\left(\frac{R + h'}{R + h_r}\right)^2 = \left(1 + \frac{h' - h_r}{R + h_r}\right)^2$$

$$= 1 + 2\left(\frac{h' - h_r}{R + h_r}\right) + \left(\frac{h' - h_r}{R + h_r}\right)^2$$

In most cases, $h' - h_r \ll R + h_r$, as shown in Figure 5. The squared term is smaller than the linear term, therefore

$$\left(\frac{R + h'}{R + h_r}\right)^2 \simeq 1 + 2\left(\frac{h' - h_r}{R + h_r}\right) \tag{2-15}$$

When Equation (2-15) is used, Equation (2-14) ean be rewritten

$$f = \frac{f_v \sec \phi_o}{\sqrt{1 - 2\left(\frac{h' - h_r}{R + h_r}\right) \tan^2 \phi_o}} \tag{2-16}$$

Equations (2-16) and (2-5) differ only by the factor $1/\sqrt{1 - 2\left(\frac{h' - h_r}{R + h_r}\right) \tan^2 \phi_o}$ which has been called the "correction factor," k.

$$k = \frac{1}{\sqrt{1 - 2\left(\frac{h' - h_r}{R + h_r}\right) \tan^2 \phi_o}} \tag{2-17}$$

The behavior of k is made explicit by using some typical values of both h' and h_r

and calculating k as a function of ϕ_o. The value of sec ϕ_o can be obtained from Figure 5. Simple geometry yields the expression,

$$\sec \phi_o = \frac{\sqrt{2R(R+h')\left[1-\cos(d/R)\right] + h'^2}}{h' + R\left[1 - \cos(d/R)\right]} \qquad (2\text{-}18)$$

which shows that ϕ_o is a function of transmission distance. Thus k increases with the transmission distance, if h' and h_r are kept constant. The correction factor k is plotted versus transmission distance in Figure 6. Sporadic E transmission is typically not greater than 1500 km, and a realistic value of k for sporadic E is between 1.000 and 1.042.

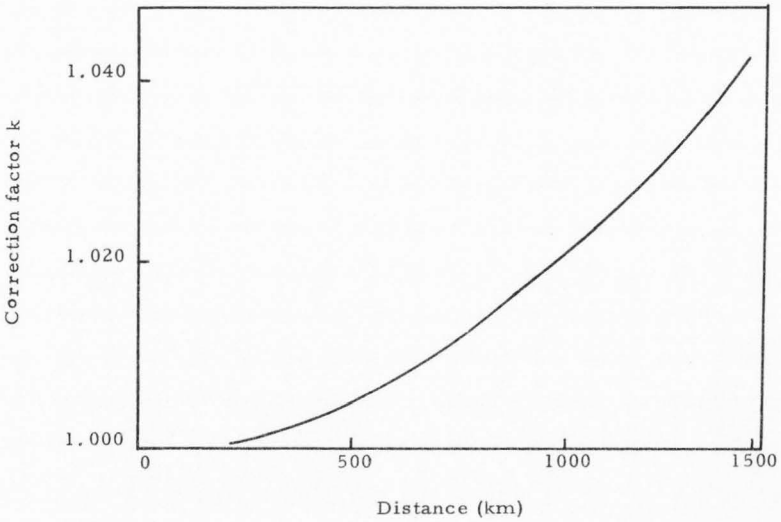

Figure 6. Variation of correction factor k with distance. [3, p. 170]

CHAPTER III

DATA ANALYSIS

It is necessary to calculate the equivalent E_s parameters, as observed from Tokyo and Wakkanai, to determine whether each E_s patch can be theoretically seen by the backscatter sounders. This analysis is accomplished by calculating the equivalent oblique frequencies corresponding to f_oE_s and f_bE_s. The critical frequency, f_oE_s, is the frequency difference, $fE_s - f_H/2$, where fE_s is the top reflection frequency from E_s and f_H is the gyrofrequency. Usually f_H is small and f_oE_s is essentially the highest frequency that will be reflected from E_s. The blanketing frequency, f_bE_s, is the highest E_s frequency below which no echos from higher altitude ionization can be seen. For $f > f_bE_s$ the E_s patch becomes partially transparent. The value of f_oE_s is always greater than or equal to f_bE_s. Accordingly, the following frequencies are defined:

$$f_{oW} = k_W(f_oE_s) \sec \phi_W$$

$$f_{bW} = k_W(f_bE_s) \sec \phi_W$$

$$f_{oT} = k_T(f_oE_s) \sec \phi_T$$

$$f_{bT} = k_T(f_bE_s) \sec \phi_T$$

where ϕ_W and ϕ_T are the incident angles from Wakkanai and Tokyo, and k_W and k_T are the correction factors for Wakkanai and Tokyo, respectively. The

locations of the three ionospheric sounders, Wakkanai, Tokyo, and Akita, in Japan, are shown in Figure 7. All of the sounders survey the common area shown over Akita. The circular area observed by the Akita VI has the appearance of a rectangle, 300 km in range and 20 degrees in azimuth on the B-scan BS photos. For purposes of analysis, whenever one-fourth or more of this area was covered by a BS E_s echo, sporadic E was assumed to be located over Akita. In other words, the BS sounder could see an E_s patch over Akita. The frequencies, f_{oW}, f_{bW}, f_{oT}, and f_{bT}, are calculated from the Akita VI data, and compared with the operating frequencies of the BS sounders at Tokyo and Wakkanai.

Data sample

The data analyzed consisted of BS records from Wakkanai and Tokyo, taken every half hour, and sporadic E parameters deduced from VI data recorded hourly at Akita. Data were analyzed for only the summer months, July and August of 1963 and June and July of 1964. These months were periods of intense E_s activity when a large percentage of useful data was available from the three stations. Table 1 shows the availability of useful data.

Table 1. Percentage of total data that was useful

Month	Akita	Wakkanai	Tokyo
July (1963)	95	51	97
August (1963)	99	87	76
June (1964)	93	94	96
July (1964)	96	73	94

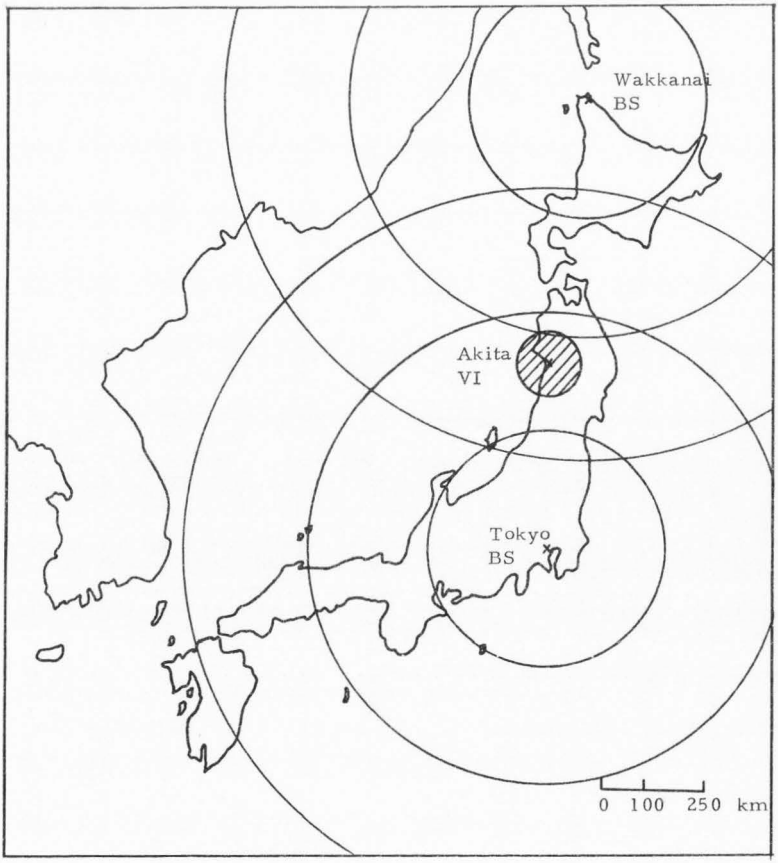

Figure 7. The sounder locations and the sky area under observation.

Data reduction errors

The accuracy of this analysis depends upon the accuracy of the sporadic E data. A number of features which effect data accuracy, are:

(1) Ground distance vs slant distance: The range of the E_s patches is assumed to be the ground distance from the transmitter to a point under the patch. In fact, the slant distance to the E_s patch over Akita, assuming 110 km height, exceeds the ground distance by 1.24 percent from Wakkanai and 2.64 percent from Tokyo. Normally these errors are negligible.

(2) Patch lengthening: An E_s patch is lengthened in range on the B-scan photo at the far edge because of the pulse duration. In the present analysis the usual pulse duration was 1 ms, which resulted in an apparent patch elongation of 150 km. The far range of E_s patches was reduced by 150 km to minimize this error.

(3) Antenna widening: The wide horizontal beam of the BS antennas causes the E_s patch to appear wider than its actual size. Although this phenomenon is a source of considerable error, no method for estimating the magnitude of this effect is available. Sporadic E patches are power-sensitive and the actual widening depends on both the power intensities incident on E_s layers and the electron densities of the patches. It is impossible to know or calculate the relative proportions of these two effects for a particular patch.

(4) Errors in reading sizes and positions of E_s patches: Errors of judgment associated with the reduction of sizes and positions of E_s patches from the BS photos to numerical form are approximately 50 km in range and

7.5 degrees in azimuth from Wakkanai. The same errors on the photos from Tokyo are estimated to be 50 km and 5 degrees.

(5) Correction factor k in the secant law: The values of the correction factor, k, in Equation (2-17) are $k_W = 1.034$ for Wakkanai and $k_T = 1.017$ for Tokyo, corresponding to 1290 km and 910 km ground transmission distances, respectively.

(6) Accuracy for published sounder data: All E_s parameters recorded by the Akita VI sounder are subject to the errors; $\pm$ 2.5 km for $h'E_s$, $\pm$ 0.05 MHz for f_oE_s, and $\pm$ 0.05 MHz for f_bE_s. Substitution of these VI errors into the secant relationship gave values of $\pm$ 1 MHz for f_{oW}, f_{oT}, f_{bW}, and f_{bT}.

(7) Probable VI antenna pattern: The half-power beamwidth of the VI antenna is approximately 30 degrees. If the medium value of $h'E_s$, 110 km, is taken as a usual height, the sky area observed by Akita would be a circle with a radius of about 30 km.

The possible data errors in the equivalent oblique frequencies provide a technique to test the secant law. For example, whenever

$$(f_{oW} - 1) > 27.7 \text{ MHz (the BS frequency)}$$

the BS sounder at Wakkanai theoretically should be able to see an E_s patch over Akita. On the other hand, whenever

$$(f_{oW} + 1) < 27.7 \text{ MHz}$$

E_s should not be seen, at least theoretically, by the Wakkanai BS sounder.

Similarly when

$$(f_{oT} - 1) > 27.7 \text{ MHz}$$

E_s over Akita should be seen by Tokyo while if

$$(f_{oT} + 1) < 27.7 \text{ MHz}$$

the Tokyo BS should not be able to see an E_s patch over Akita. The secant law was considered reliable in the application to E_s layer if any of the above conditions were satisfied and E_s was in fact recorded as assumed. The secant law was considered unreliable for those cases in which the above relationships were met but E_s was not recorded as anticipated.

It is difficult to compare f_{bW} and f_{bT} with 27.7 MHz since f_{bW} and f_{bT}, except in rare cases, were normally much lower than 27.7 MHz.

Visibility of sporadic E by backscatter sounder

"Visibility" is a measure of the ability of a BS sounder to observe an E_s patch when this patch is in the area surveyed by the sounder. There is ample evidence (7) that the two BS sounders observing the same E_s patch do not see the same thing. It is desirable, therefore, to note and discuss some of the features which will effect the recording of sporadic E. These features are:

the sensitivity of the BS sounder receiver;

the power density incident on E_s patches, which depends upon the distances between sounder and patches and the transmitted power;

the equivalent oblique frequency, which includes the effect of sounder-patch distances and a possible tilt angle of the E_s patch; and

the ground scattering coefficient, which depends upon terrain type and profile.

The backscatter sounders at Wakkanai and Tokyo are identical equipment and both BS stations are so located geographically relative to Akita that their respective backscattering areas are composed of half portions of land and sea.

Four individual areas under simultaneous survey of both BS sounders are shown in Figure 8. The symmetry of this geometry accentuates any differences in sounder performances. These four circular areas, with radii of 80 km each and located at points equidistant from the Wakkanai and Tokyo BS stations, appeared as approximately four rectangular areas on the B-scan photos of each BS sounder. Each rectangle was approximately 25 degrees in azimuth and 400 km in range. An E_s patch was assumed to be located in one of the areas whenever one-fourth or more of the corresponding B-scan rectangular area was covered by E_s return. The E_s returns received by Wakkanai from areas A, B, C and D, are designated AW, BW, CW and DW, respectively, and AT, BT, CT and DT designate E_s returns received by Tokyo in Table 2. Since the ground scattering areas are both at sea, the ratios CT/CW and DT/DW indicate that the visibility of E_s from Tokyo was much better than that of Wakkanai. This fact implies that the gain of the Tokyo system was greater or that perhaps the E_s patches were tilted upward to the north.

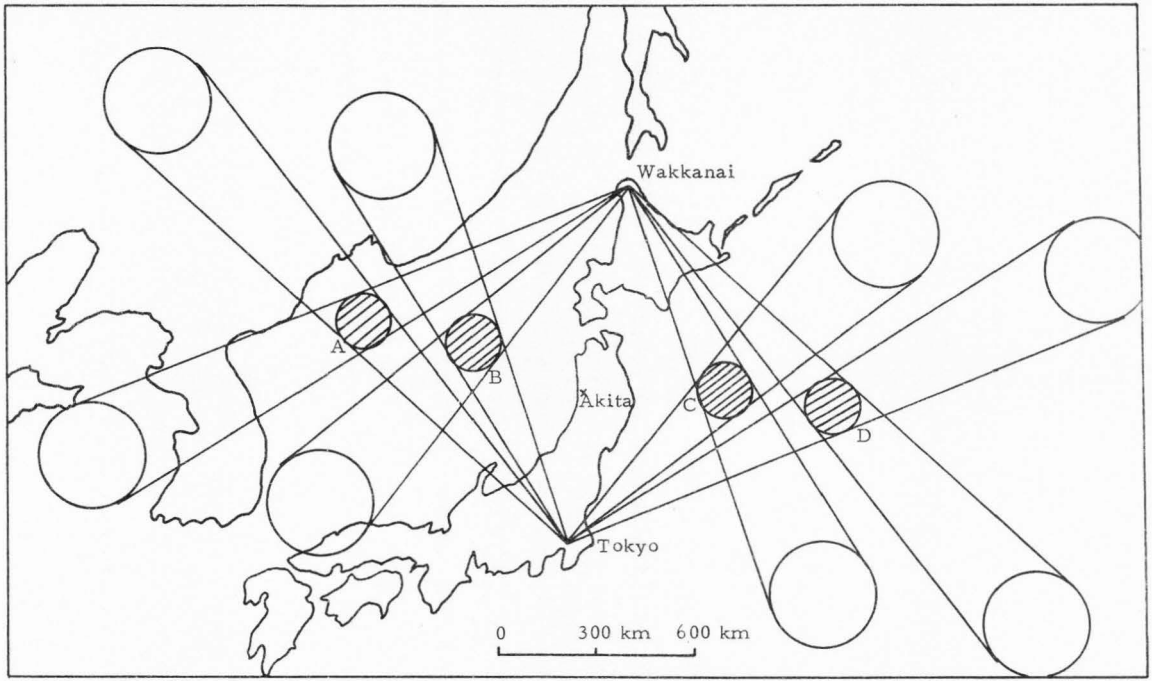

Figure 8. Four areas simultaneously observed by Wakkanai and Tokyo BS sounders and their respective backscattering areas.

Table 2. E_s returns received by BS stations during June and July of 1964 from areas A, B, C, D of Figure 8

No. of E_s returns received by T(Tokyo) and W(Wakkanai) from areas A, B, C, D	AT	AW	BT	BW	CT	CW	DT	DW
	266	273	759	309	863	407	571	107

	AT/AW	BT/BW	CT/CW	DT/DW
Ratio	1:1	2.5:1	2.1:1	5.3:1

Because areas B and C are closer to the BS stations than areas A and D, the power densities should be stronger at B and C and more E_s echos could be expected from B and C than from A and D. On the other hand, the incidence angle is greater at A and D, hence according to the secant law, if it holds for E_s, more E_s from A and D are expected. The percentages of E_s returns from each area are shown in Figure 9. Since E_s returns to each sounder from B and C exceed the returns from A and D, it is concluded that the visibility of E_s by backscatter sounder is heavily dependent on the power density incident on E_s patch.

The comparison of observations of BS sounders and measurements of VI sounder

With the factors that effect BS visibility of E_s patches in mind, the results of the 1963 and 1964 data can now be examined. Comparisons between VI and BS were possible only when Akita VI recorded an E_s patch, since the BS

Total numbers of E_s returns from A, B, C, D to each sounder

Wakkanai: 1096
Tokyo: 2459

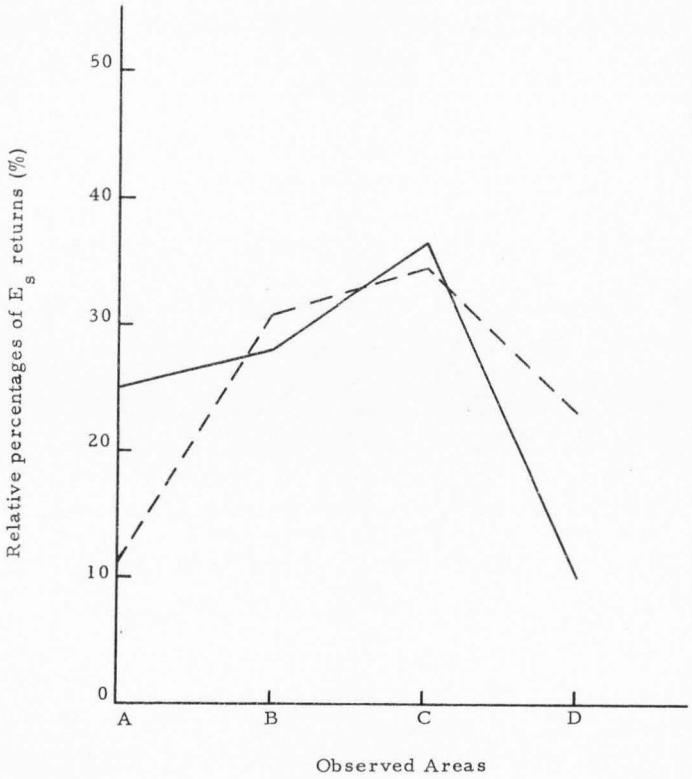

Figure 9. Percentage E_s return from observed areas shown in Figure 8.

sounder could not possibly see an E_s patch over Akita unless sufficient ionization was present. It must be recognized at the outset that considerably more E_s was "seen" by the VI than the BS sounders. Furthermore, the comparison could be made only when VI was "comparable" with at least one BS. To be "comparable," the following two conditions had to be satisfied simultaneously: (1) a clear, readable, operational B-scan photo from the BS station had to be available at the particular hour, and (2) the fixed frequency of BS, $f_x = 27.7$ MHz, should be either greater than $f_{oT,\ oW} + 1$ or less than $f_{oT,\ oW} - 1$. Cases in which $f_{oT,\ oW} - 1 < f_x < f_{oT,\ oW} + 1$ are indeterminate owing to reading error of the VI ionograms.

The values for the Wakkanai and Tokyo BS sounders for July of 1963 are given in the first two rows of Table 3 and will be discussed in detail to show the results of the comparison study. Values for the other months are similar. In Column 1 the value, 337, represents the total number of hours in the month when the Akita VI recorded an E_s patch overhead and the VI was "comparable" with Wakkanai BS. There were 26 hours (Column 2) of a possible 337, when Wakkanai saw the E_s patch over Akita. "Visibility" of Wakkanai BS, the quotient (26/337), was very poor--7.71 percent, as shown in Column 3. The reason for the poor "visibility" was that the fixed frequency, 27.7 MHz, used by the Wakkanai BS was too high to be reflected by most of the E_s patches ($f_{oW} + 1 < f_x$). This fact is reflected by the values in Columns 6 and 7. Sporadic E densities theoretically strong enough to reflect BS signals are given in Columns 4 and 5. The percentage in Column 8 represents theoretically predicted

Table 3. Comparison of E_s observations from Wakkanai (W) or Tokyo (T) BS, and Akita VI

Month (year)	BS	(1) Total No. of hours (E_s seen by VI)	(2) Total No. of hours (E_s seen by BS)	(3) Real visibility of BS (%)	(4) No. of hours (E_s seen by BS) when $f_{oW}, oT^{-1} > f_x$	(5) No. of hours (E_s not seen by BS) when $f_{oW}, oT^{-1} > f_x$	(6) No. of hours (E_s seen by BS) when $f_{oW}, oT^{+1} < f_x$	(7) No. of hours (E_s not seen by BS) when $f_{oW}, oT^{+1} < f_x$	(8) Theoretical visibility of BS (%)	(9) Reliability of secant law (%)
July (1963)	W	337	26	7.71	12	55	14	256	19.9	79.5
	T	668	138	20.7	59	18	79	512	11.5	85.4
August (1963)	W	595	11	1.85	8	98	3	486	17.8	83.0
	T	519	40	7.71	26	20	14	459	8.87	88.4
June (1964)	W	623	87	14.0	77	133	10	403	33.7	77.0
	T	633	228	36.0	118	8	110	397	19.9	81.3
July (1964)	W	500	25	5.0	21	114	4	361	27.0	76.4
	T	655	195	29.8	95	8	100	452	15.7	83.5

"visibilities" obtained by dividing Columns 4 and 5, the number of hours when $f_{oW} - 1 > f_x$, by the total number of data, as shown in Column 1. Theoretical "visibilities" were somewhat different from the real "visibilities" shown in Column 3. For Wakkanai the theoretical visibility was greater than the real visibility while for Tokyo the situation was reversed. Similar results were found in all months, except for Tokyo in August of 1963. A possible reason that Wakkanai saw fewer E_s patches over Akita while Tokyo saw more E_s patches than were theoretically predicted by the secant law might be a tilt in the E_s layer upward to the north. This situation reduces the effective incident angle from Wakkanai and decreases the probability that E_s will be seen from Wakkanai. The opposite situation simultaneously occurs at Tokyo. Some evidence similar to that shown in Figure 10 supports a hypothesis of a 2 degree tilt to the north. On the other hand it has already been seen and surmised that the reflection of a radio wave from an E_s patch is heavily dependent on the incident power, and the Tokyo BS sounder has greater system gain, therefore it records more E_s; although it is difficult to explain more E_s than theory predicts, as shown in Column 6.

The values in Columns 4 and 7 are those hours in which the observed results from Wakkanai BS are in accordance with the secant law prediction. Column 9 reflects this data by estimating the reliability of the secant law, i.e., the percentage of time the secant law is not invalid. The reliability of the secant law is over 75 percent for all data, with the Tokyo figures generally 5 percent greater than the corresponding Wakkanai values.

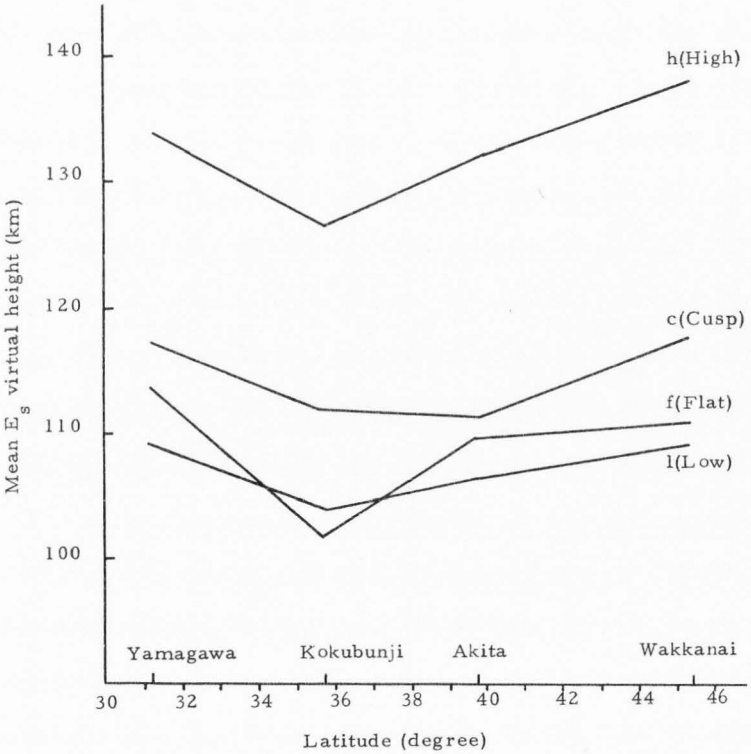

Figure 10. Mean h'E_s vs. latitude for temperate E_s types July, 1962. [5, p. 47]

Two items which have an effect on the reliability of the secant law are: (1) the power gain of the sounder system, and (2) a scattering phenomenon which can take place, especially when a sporadic E event is just commencing or ending. The Wakkanai values in Column 5 are uniformly much larger than the corresponding Tokyo values. Since it has been shown that the Tokyo BS sounder had a higher system gain and Tokyo values are lower in Column 5, it is logical to attribute a large percentage of Column 5 to lack of transmitter power or system gain. The situation can be described by presuming that the transmitted energy was reflected from the E_s patch but that the resulting echo was too weak to be detected.

Theoretically, no cases of sporadic E should be recorded in Column 6 but in fact, Tokyo BS recorded a large number of E_s patches. Since the theory pertains to specular reflection and does not hold for inhomogeneous plasmas, it is attractive to attribute the occurrences represented by Column 6 to a strong E_s scattering phenomena. If the values of Columns 5 and 6 could be reduced by appealing to arguments similar to those above, the reliability of the secant law would have an even higher value. Only f_oE_s was considered in the E_s occurrence statistics presented in Table 3.

In Figures 11 and 12, the reliability of the secant law is plotted against the difference of $f_oE_s - f_bE_s$. These figures show that for both BS stations the secant law is more reliable for the small values of $f_oE_s - f_bE_s$ and is less reliable with the increase of $f_oE_s - f_bE_s$.

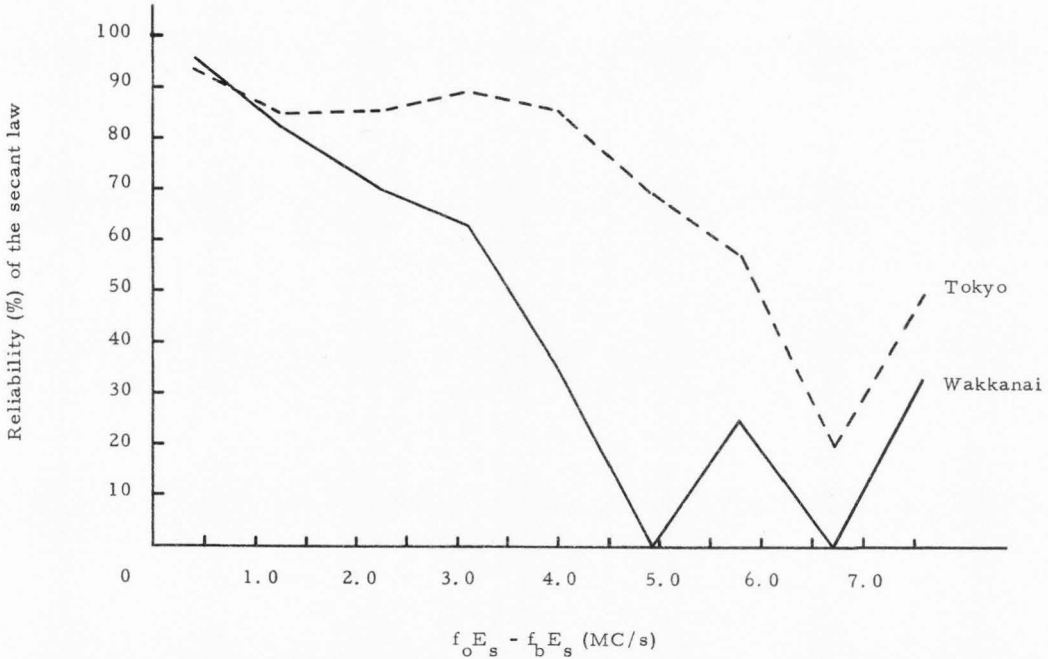

Figure 11. Reliability of the secant law vs. $f_oE_s - f_bE_s$, July and August of 1963.

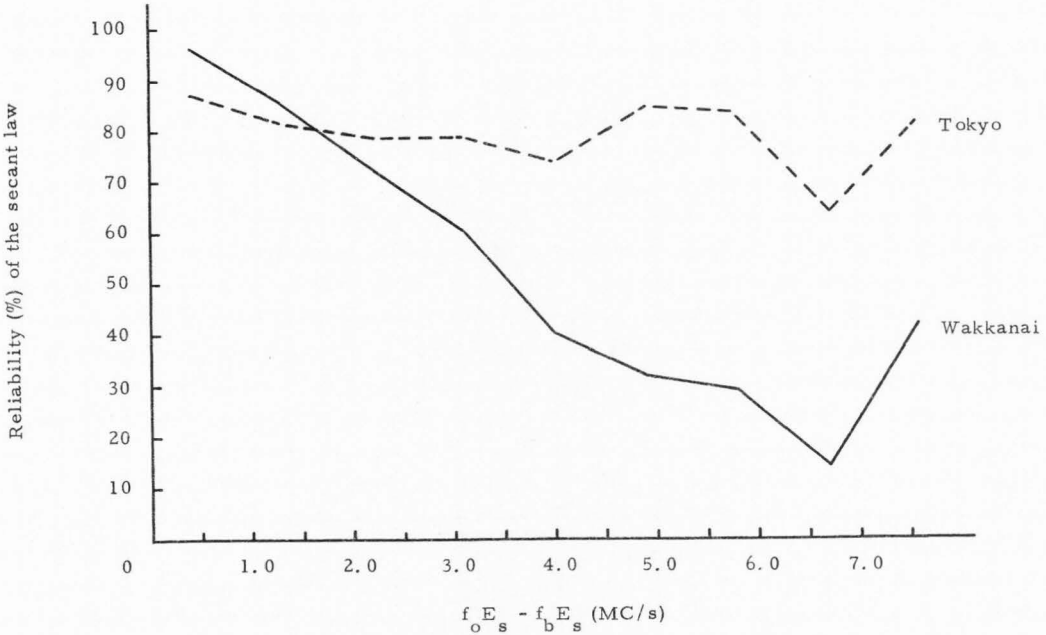

Figure 12. Reliability of the secant law vs. $f_oE_s - f_bE_s$, June and July of 1964.

Figures 13, 14, 15, and 16 illustrate the statistical distribution of VI data plotted as the number of occurrences of each class of $f_o E_s - f_b E_s$ for July and August of 1963 and June and July of 1964. Only VI data that was "comparable" with BS sounder, were used. These figures indicate that most E_s patches had small values of the difference of $f_o E_s - f_b E_s$. Note that the histograms are in the form of a decreasing exponential function.

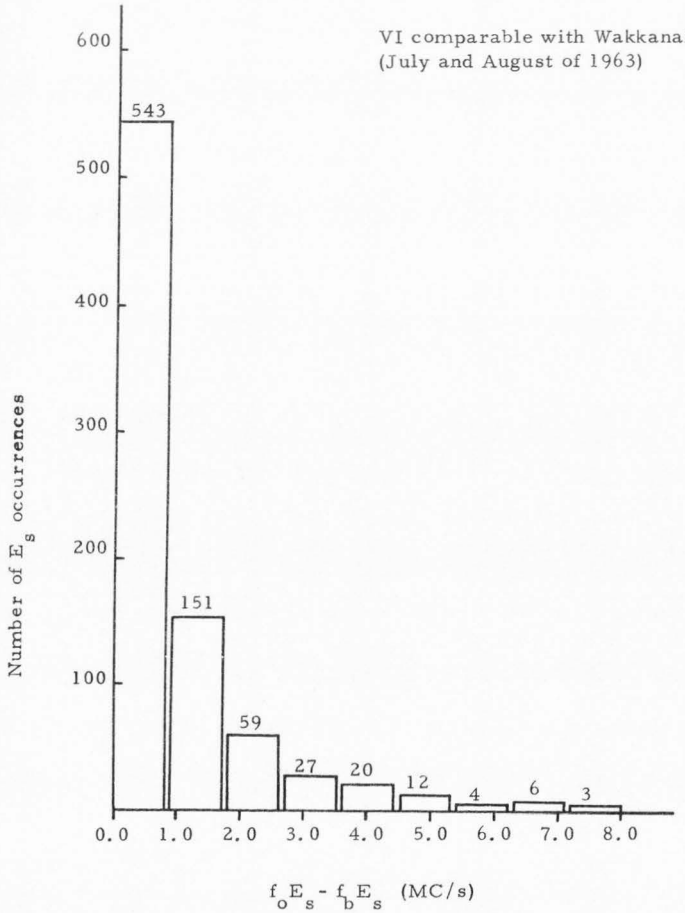

Figure 13. Sporadic E occurrences versus $f_oE_s - f_bE_s$.

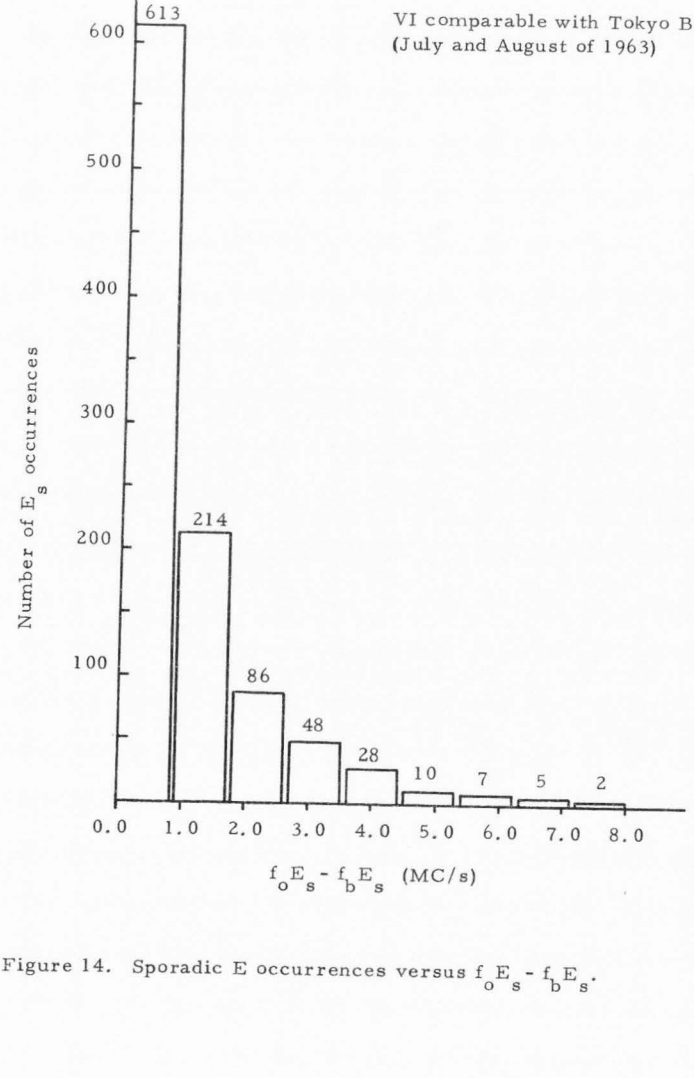

Figure 14. Sporadic E occurrences versus $f_oE_s - f_bE_s$.

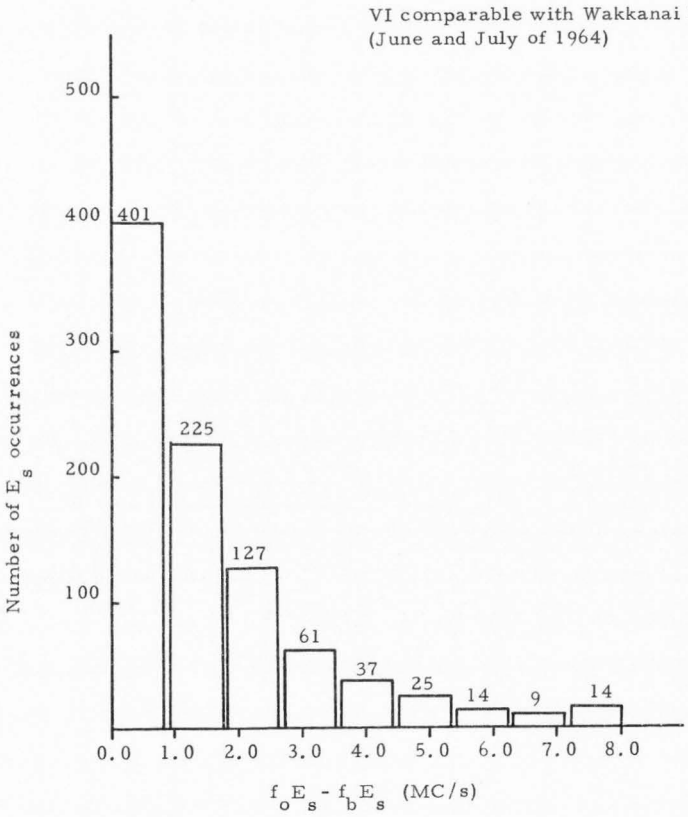

Figure 15. Sporadic E occurrences versus $f_oE_s - f_bE_s$.

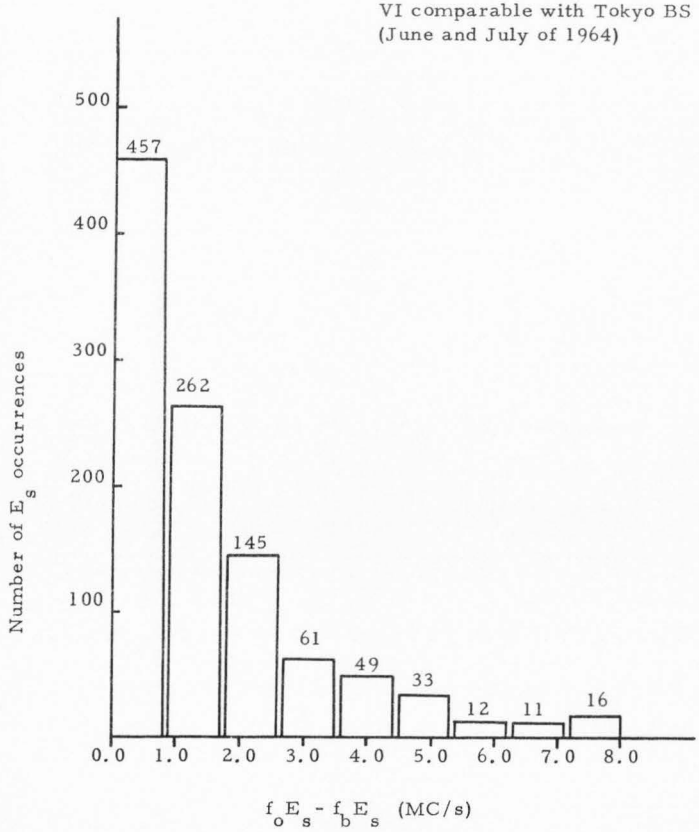

Figure 16. Sporadic E occurrences versus $f_o E_s - f_b E_s$.

CHAPTER IV

SPORADIC E MODELS

Two sporadic E models were suggested by Reddy to explain the E_s frequency characteristics (8).

Model I

This model supposes an E_s layer with uniform horizontal electron density. A radio wave with frequency below the maximum plasma frequency of the layer will be totally reflected. The reflection will obey the secant law, as shown already in Chapter II. At frequencies above the maximum plasma frequency the wave can penetrate through the E_s patch. If the electron density gradient is sufficiently sharp, some energy can be reflected. This phenomenon is called partial reflection. The maximum plasma frequency in this model is called f_bE_s and f_oE_s is the top frequency detected by the receiver due to the partial reflection mechanism. Four model layers which might be used for sporadic E to permit the calculation of partial reflection are shown in Figure 17. The reflection coefficient is defined as the ratio of the signal strength of a reflected wave to that of an incident wave. The coefficients of partial reflection for vertical and oblique incidences can be shown to be the same if the oblique and vertical frequencies are related by the secant law. According to Budden (2), the magnitude of the reflection coefficient for the linear electron profile in (a) of Figure 17 is given below:

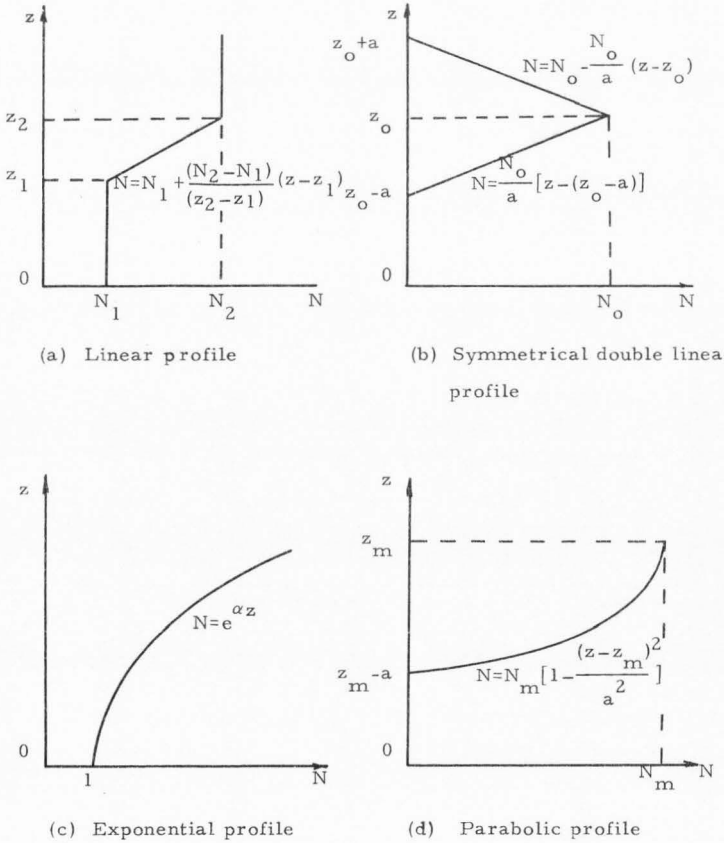

(a) Linear profile

(b) Symmetrical double linear profile

(c) Exponential profile

(d) Parabolic profile

Figure 17. Four profiles of electron density of Model I.

$$|R| = \left| \frac{\begin{vmatrix} iuq_2 A_i(\zeta_2) + A_i'(\zeta_2) & iuq_2 B_i(\zeta_2) + B_i'(\zeta_2) \\ iuq_1 A_i(\zeta_1) + A_i'(\zeta_1) & iuq_1 B_i(\zeta_1) + B_i'(\zeta_1) \end{vmatrix}}{\begin{vmatrix} iuq_2 A_i(\zeta_2) + A_i'(\zeta_2) & iuq_2 B_i(\zeta_2) + B_i'(\zeta_2) \\ -iuq_1 A_i(\zeta_1) + A_i'(\zeta_1) & -iuq_1 B_i(\zeta_1) + B_i'(\zeta_1) \end{vmatrix}} \right| \quad (4\text{-}1)$$

where

$$q_1^2 = \cos^2\phi_o - \left(\frac{\omega_1}{\omega}\right)^2$$

$$q_2^2 = \cos^2\phi_o - \left(\frac{\omega_2}{\omega}\right)^2$$

$$u = \left[\frac{(z_2 - z_1)}{c(\omega_2^2 - \omega_1^2)}\right]^{1/3} \omega$$

$$\zeta_1 = -q_1^2 u^2$$

$$\zeta_2 = -q_2^2 u^2$$

c = velocity of light in free space,

ω_1, ω_2 = the angular plasma frequencies corresponding to the electron densities N_2 and N_1, respectively,

ω = the angular frequency of the incident radio wave,

A_i, B_i, A_i' and B_i' = the Airy functions and their respective derivatives,

ϕ_o = incident angle.

The reflection coefficients for vertical and oblique incidences will be the same if uq_1 and uq_2 for both vertical and oblique incidences are equal. These equalities can be written as

$$\omega_o\left[\cos^2\phi_o - \left(\frac{\omega_1}{\omega_o}\right)^2\right]^{1/2} = \omega_v\left[1 - \left(\frac{\omega_1}{\omega_v}\right)^2\right]^{1/2}$$
$$\omega_o\left[\cos^2\phi_o - \left(\frac{\omega_2}{\omega_o}\right)^2\right]^{1/2} = \omega_v\left[1 - \left(\frac{\omega_2}{\omega_v}\right)^2\right]^{1/2} \qquad (4\text{-}2)$$

where ω_o, ω_v = the angular frequencies of oblique and vertical incidences. Either equation of (4-2) can be reduced directly to the form of the secant law, $f_o = f_v \sec \phi_o$. In a similar way, the secant law can also be proved true for the symmetrical double linear profile, the exponential profile, and the parabolic profile of Figure 17.

Figure 18 shows the coefficient of partial reflection versus frequency for the linear electron profile. Note the similarity between this figure and the distributions of E_s occurrences versus $f_oE_s - f_bE_s$ in Figures 13 through 16.

Model II

This E_s model is not homogeneous as is the previous case, but has irregularities in the ionization in the horizontal and vertical directions. Two subcases might be considered: One, the irregularities are so great and random that there is no formula which can describe the feature of the E_s layer. The secant law will probably not hold true in this case.

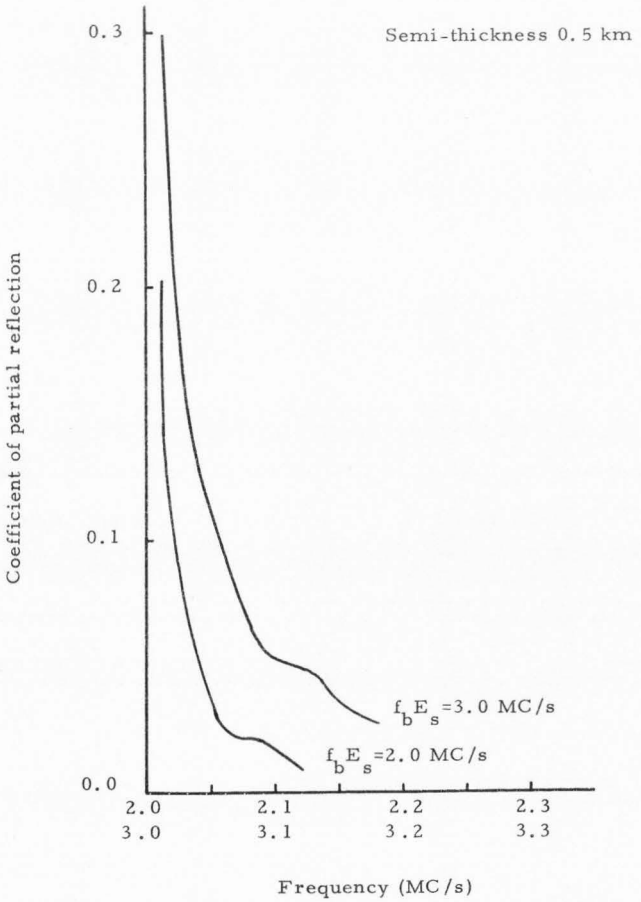

Figure 18. Coefficient of partial reflection vs. frequency ($f > f_b E_s$).

The values of f_bE_s and f_oE_s correspond respectively to the lowest overall value of electron density and the peak electron density found in the ionospheric volume under observation. The area surveyed by a VI sounder might be composed of "holes" with less densities and "blobs" with greater densities. The blanketing frequency (f_bE_s) will be reflected from both holes and blobs, (i.e., complete reflection from the E_s layer). As the frequency is increased above f_bE_s, part of the wave energy passes through some of the holes producing echoes from the F region. When the frequency is increased so that the wave is nowhere reflected from the ionization, its value is f_oE_s.

In the other case, the irregularities are small-scale, i.e., they have a fractional deviation of only 5 to 10 percent from the ambient average electron concentration. The scale size of these irregularities is 10 to 100 meters. The phenomenon of scattering exists for any frequency. The blanketing frequency, f_bE_s, corresponds to the plasma frequency of maximum ambient average electron concentration. The critical frequency, f_oE_s, is approximately the top frequency of the returned signal due to scattering.

The volume scattering due to small-scale irregularities can be handled by a theory formulated by Booker (1). The scattering coefficient is defined as the ratio of the power scattered per unit solid angle in some direction under consideration to the incident power density. Under the assumption that the magnetic field is unimportant and the irregularities are anisotropic, the scattering coefficients are given as

$$\sigma_1 = (2\pi)^{3/2} r_e^2 \overline{(\triangle n)^2} \cdot \sin x \cdot (abc) \cdot \exp\left\{-\left[2\pi^2/\lambda_m^2\right]\left[a^2 (l_1 - l_2)^2 + b^2 (m_1 - m_2)^2 + c^2 (n_1 - n_2)^2\right]\right\} \quad (4\text{-}3)$$

and

$$\sigma_2 = \frac{8\pi r_e^2 \overline{(\triangle n)^2} \sin^2 x \cdot (abc)}{\left\{1 + \left[4\pi^2/\lambda_m^2\right]\left[a^2 (l_1 - l_2)^2 + b^2 (m_1 - m_2)^2 + c^2 (n_1 - n_2)^2\right]\right\}^2} \quad (4\text{-}4)$$

corresponding to the spatial auto-correlation functions

$$p_1(x, y, z) \propto \exp\left[-\frac{1}{2}\left(\frac{x^2}{a^2} + \frac{y^2}{b^2} + \frac{z^2}{c^2}\right)\right]$$

and

$$p_2(x, y, z) \propto \exp\left[-\left(\frac{x^2}{a^2} + \frac{y^2}{b^2} + \frac{z^2}{c^2}\right)^{1/2}\right]$$

respectively,

where

r_e = the classical radius of the electron,

$\overline{(\triangle n)^2}$ = the mean square departure of electron density,

x = the angle between the direction of scattering and the direction of the electric field at the scattering point, here assumed to be $\pi/2$,

a, b, c = the scale lengths of the irregularities in three directions, x, y, and z respectively,

λ_m = the mean wavelength of the radio wave in the medium,

(l_1, m_1, n_1) = the direction numbers of the incident direction,

(l_2, m_2, n_2) = the direction numbers of the scattering direction under consideration.

A geometry of vertical and oblique incidences and the respective scattering geometry are shown in Figure 19.

If the scattering coefficient for the vertical incidence σ_v and that for the oblique incidence σ_o are set equal, the equation $\sigma_o = \sigma_v$, by using either σ_1 of Equation (4-3) or σ_2 of Equation (4-4) on both sides, can be reduced to the simple form

$$\frac{1}{\lambda_{mo}} \cos \phi_o = \frac{1}{\lambda_{mv}} \tag{4-5}$$

where

ϕ_o = the incident angle,

$\lambda_{mv}, \lambda_{mo}$ = the mean wavelengths in the medium, of the vertical and oblique incidences, respectively.

Equation (4-5) can be rewritten as

$$f_o = f_v \sec \phi_o \left(\frac{\epsilon_v}{\epsilon_o}\right)^{\frac{1}{2}} \tag{4-6}$$

by using

$$\lambda_{mo} = \frac{\lambda_o}{(\epsilon_o)^{1/2}}$$

$$\lambda_{mv} = \frac{\lambda_v}{(\epsilon_v)^{1/2}}$$

where

λ_v, λ_o = the wavelengths in free space, of the vertically and obliquely incident waves, respectively,

ϵ_v, ϵ_o = the permittivities in the medium, of the vertically and obliquely incident waves, respectively.

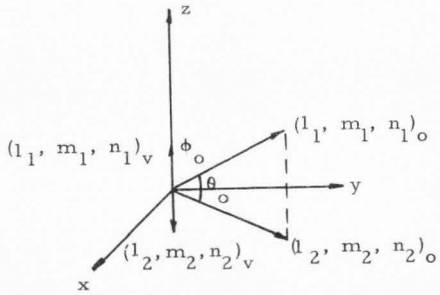

$$\text{vertical incidence} = (l_1, m_1, n_1)_v = (0, 0, 1)$$

$$\text{scattering of vertical incidence} = (l_2, m_2, n_2)_v = (0, 0, -1)$$

$$\text{oblique incidence} = (l_1, m_1, n_1)_o = \left(0, \cos\frac{\theta_o}{2}, \sin\frac{\theta_o}{2}\right)$$

$$\text{scattering of oblique incidence} = (l_2, m_2, n_2)_o = \left(0, \cos\frac{\theta_o}{2}, -\sin\frac{\theta_o}{2}\right)$$

Figure 19. Geometry of vertical and oblique incidences of radio waves and their respective scattering directions under consideration.

Equation (4-6) has one more factor, $\left(\frac{\epsilon_v}{\epsilon_o}\right)^{1/2}$, compared with the secant law $f_o = f_v \sec \phi_o$. This factor is approximately unity only when both the frequencies of vertically and obliquely incident waves are much greater than the plasma frequency of the medium. For the case of sporadic E under consideration, this condition is not true. Therefore, the secant law does not hold in the case of small-scale irregularities for frequencies near the plasma frequency.

CHAPTER V

SUMMARY AND CONCLUSION

The results of the data analysis can be summarized as follows:

1. The secant law for sporadic E was not invalid 75 percent of the time that the VI and BS data were comparable. This negative conclusion is necessitated by the fact that a great number of sporadic E occurrences were not sufficiently dense to be recorded on the 27.7 MHz backscatter sounders. Most of the time 27.7 MHz was greater than the oblique equivalent critical frequency calculated by the secant law.

2. The secant law was more reliable for prediction of E_s echos when the values of the differences of $f_oE_s - f_bE_s$ are small. This fact seems to imply that the smaller the values of $f_oE_s - f_bE_s$, the more regular the E_s layer. Approximately 75 percent of the sporadic E occurrences had $f_oE_s - f_bE_s$ less than 2 MHz.

3. The statistical distribution of the E_s occurrences versus $f_oE_s - f_bE_s$ showed some similarity to the curve of the partial reflection coefficient versus frequencies above f_bE_s. This similarity might provide support for the contention that the partial reflection is responsible for f_oE_s.

Sporadic E Model I discussed in Chapter IV, supposes a uniform horizontal strata of electrons. It was shown that for this model, the secant law was valid for total reflection, the radio wave frequency $f < f_bE_s$, and the

partial reflection, $f > f_b E_s$, where $f_b E_s$ corresponds to the maximum plasma frequency. Sporadic E Model II had vertical and horizontal irregularities like lumpy pudding. The secant law was shown theoretically to fail for this model. Therefore, in a rigorous experimental verification of the secant law for sporadic E, effort should be made to distinguish between the E_s echos predicted by Models I and II.

The blanketing frequency, $f_b E_s$, corresponds to the maximum plasma frequency and it should be used to verify the validity of the secant law for total reflection. Since it seems impossible for a BS sounder to measure accurately the oblique blanketing frequency or to distinguish the E_s echos of total reflection from those of partial reflection, an oblique ionosonde is suggested to replace the BS sounder. The two ionosondes, one vertical and the other oblique, are oreinted to survey a common area of sky simultaneously, as shown in Figure 20. The validity of the secant law for total reflection could then be determined by comparing the oblique blanketing frequency measured by the oblique ionosonde with the blanketing frequency measured by the vertical ionosonde.

The reflection coefficient for $f > f_b E_s$ can be calculated by measurement of E_s at three different frequencies. The signal strength of a radio wave will depend primarily on three factors (3), which are:

(1) spatial spreading and defocusing which vary as the inverse squared relationship $\frac{c}{S_e^2}$, where c is a constant determined by the beam pattern of the radiation and S_e is the effective distance.

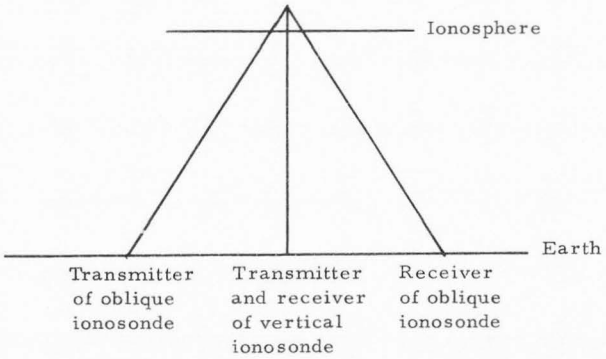

Figure 20. The ionospheric survey of one vertical ionosonde and one oblique ionosonde.

(2) Non-deviative absorption in the D region, $e^{-\int_s K ds}$, where s = ray path of propagation, and

$$K = C_K \frac{N\nu}{\omega^2 + \nu^2} \doteq C_K \frac{N\nu}{\omega^2} \quad \text{if } \omega \gg \nu$$

in which

N = electron density,

ν = collision frequency,

ω = frequency of the radio wave,

C_K = a constant.

(3) The partial reflection in an E_s layer with the magnitude of reflection coefficient represented by R.

Factor (1) is almost independent of the frequency variation of the radio wave, but factors (2) and (3) will change with the frequency. If E_T and E_R designate the field strengths of a radio wave at the transmitting antenna and the receiving antenna, respectively, E_R can be expressed in terms of E_T by

$$E_R = E_T R \left(\frac{c}{S_e^2}\right)_b \left(\frac{c}{S_e^2}\right)_a \quad e^{-\int_s K ds} \tag{5-1}$$

where the subscripts b and a represent, respectively, the parts of factor (1) before and after the reflection of E_s layer.

Three radio waves will be transmitted with the same signal strength E_T but at three different frequencies f_1, f_2 and f_3, where $f_1 < f_2 < f_b E_s$ and $f_3 > f_b E_s$. The three corresponding signals received at the receiving antenna will be recorded as E_{R1}, E_{R2} and E_{R3}. Note that for a frequency less than $f_b E_s$, R is theoretically unity. By using Equation (5-1) to calculate E_{R1}, E_{R2} and E_{R3} and then forming the ratios E_{R2}/E_{R1} and E_{R3}/E_{R2}, the coefficient of partial reflection at the frequency f_3 can be expressed in the following form

$$R = \frac{E_{R3}}{E_{R2}} \exp\left[-\left(\frac{f_1}{f_3}\right)^2 \left(\frac{f_3^2 - f_2^2}{f_2^2 - f_1^2}\right) \ln\left(\frac{E_{R2}}{E_{R1}}\right)\right] \tag{5-2}$$

The two ionosondes in Figure 20 can be arranged to perform this measurement. When these ionosondes measure the same reflection coefficient, the comparison of their corresponding frequencies will yield a verification of the validity of the

secant law for partial reflection from the E_s layer of Model I.

These measurements are based on frequencies which are sufficiently high that the earth's magnetic field can be neglected. If this condition is not valid, one must treat both the ordinary and extraordinary waves that exist in a magnetoionic plasma.

SELECTED BIBLIOGRAPHY

1. Booker, H. G. Radio scattering in the lower ionosphere. Journal of Geophysical Research, Space Physics 64:2164-2173. December, 1959.

2. Budden, K. G. Radio waves in the ionosphere, Chapters 16 and 17, pp. 319-384. Cambridge University Press, Cambridge, England. 1966.

3. Davies, Kenneth. Ionospheric radio propagation, Chapter 2, pp. 63-71; Chapter 4, pp. 159-179; Chapter 5, pp. 217-241. National Bureau of Standards Monograph 80. U. S. Government Printing Office, Washington, D.C. April 1, 1965.

4. Harris, Richard W. Validation of the secant law for sporadic-E utilizing backscatter sounder data. Utah State University, Engineering Experiment Station, Antenna and Propagation Laboratory, Special Report Number 1, Logan, Utah. 1964.

5. Harris, Richard W., Mark C. Austin, Clayton Clark, and Bruce O. Watkins. Relationships among critical frequency, virtual height, and latitude for various types of temperate-zone sporadic-E. Utah State University, Engineering Experiment Station, Antenna and Propagation Laboratory, Technical Paper, Logan, Utah. n.d.

6. Mckee, Rondal R. Land versus sea backscatter return. Utah State University, Engineering Experiment Station, Antenna and Propagation Laboratory, Special Report Number 7, Logan, Utah. 1965.

7. Painter, James N. Correlations of sporadic-E aspect sensitivity and layer tilt. Utah State University, Engineering Experiment Station, Antenna and Propagation Laboratory, Special Report Number 5, Logan, Utah. 1965.

8. Reddy, C. A. Physical significance of the E_s parameters f_bE_s, fE_s, and f_oE_s. 2. Causes of partial reflections from E_s. Journal of Geophysical Research, Space Physics 73:5627-5647. September, 1968.

9. Roundy, Carlos B. Measurement of radio backscatter coefficient. Utah State University, Engineering Experiment Station, Antenna and Propagation Laboratory, Special Report Number 6, Logan, Utah. 1965.

10. Smith, Newbern. The relation of radio sky-wave transmission to ionosphere measurement. Proceeding of the IRE 27:332-347. November, 1939.

VITA

Ruey-Yuan Han

Candidate for the Degree of

Master of Science

Thesis: A Study of the Secant Law for Sporadic E.

Major Field: Electrical Engineering

Biographical Information:

Personal Data: Born in Szechuan, China, November 4, 1942, son of Chin-Tung Han and Chan-chin Chen.

Education: Attended elementary school in Kungshan, Taiwan; graduated from Taiwan Provincial Hu-wei High School in 1960; received a degree of Bachelor of Science from Cheng-Kung University with a major in Electrical Engineering in 1965; completed requirements for Master of Science degree with a major in Electrical Engineering at Utah State University, Logan, Utah, in 1970.

Professional Experience: 1968 to present, research assistant, Antenna and Propagation Laboratory, Utah State University; 1966-1967, teacher of physics at Taiwan Provincial Chun-Inn Senior High School.